[= *

Master Degree in Physics

Master Thesis

Octupole Deformation in Sm isotopes using covariant density functional theory

Prepared by:

Sami Mukhiemer

Supervised by:

Dr. Hazem abusara

Birzeit, Palestine

January 2018

Octupole deformation for Sm isotopes using covariant density functional theory

التشوه الثماني لنظائر ساماريوم

By

Sami Hani Sami Mukhiemer

This Thesis was submitted in partial fulfillment of the requirements for the Master's Degree in physics From the Faculty of Graduate Studies at Birzeit University, Palestine

Thesis committee:

Dr. Hazem Abusara (Supervisor)

Prof. Henry Giacaman (Member)

Dr. Esmael Badran (Member)

January 2018

Octupole Deformation for Sm Isotopes Using Covariant Density Functional Theory

التشوه الثماني لنظائر ساماريوم

By

Sami Mukhiemer

Accepted by the Faculty of Graduate Studies, Birzeit University, in partial fulfillment of the degree of Master of physics

Abstract

Octupole deformations play a significant role in the rare-earth region of the nuclear chart. We will study the ground state properties in the even-even Sm isotopes, and investigate the role of octupole deformation and its effect on several ground state properties, such as binding energy, binding energy per nucleon, neutron and proton mean radii, and two neutron separation energy. For this investigation covariant density functional theory with BCS approximation for the pairing correlation will be employed.

ملخص

التشوه الثماني له دور مهم و فعّال في دراسة أنوية الذرات الأرضية، سوف ندرس في هذه الأطروحة خصائص مستوى الطاقة الأرضي لنظائر الساماريوم، سنبحث في أثر التشوه الثماني وتأثيره عل قوة الربط االنووية، وطاقة الدمج، وطاقة الجزيئات، وقد إستخدمنا في الأطروحة نظرية كثافة الدالة، التي أثبتت فعاليتها في التعامل مع هذه النوعية من المسائل.

لقد درسنا تأثير التشوه الثماني على قوة الربط النووية، وقوة الربط النووية لكل نيكليون، كما ودرسنا تأثيره على الخصائص الفيزيائية للنوة مثل أنصاف أقطار النيوترونات وأنصاف أقطار البروتونات، وقد تمت هذه الأبحاث على نضائر الساماريوم التي عدد برتوناتها وعدد نيوتروتها زوجي.

Acknowledgement

First of all, I thank Allah for giving me the power to believe in my passion and pursue my dreams.

A very special thanks to Dr. Hazem Abusara for being my first supervisor and giving me the opportunity to do this thesis, as well as for his help, care and support.

A big thank to him for the time he gave to me and answering all my questions in physics and in programming. Also I want to thank all the graduate students at Birzeit University, for many useful and productive discussions I had with them.

To prof. Henry Giacaman, and Dr. Esmael Badran for being part of the thesis defense, reading and assessing. Beside to being my teachers and giving me a lot of information over the last six years. As well as many other teachers at Birzeit university in my Bachelor and Master studies.

Dedication

Heartiest thanks for my friends, especially my close friends. I want to send my warm and sincere to my parents for their support throughout all over the years in my life. To my wife Lamees that it always beside me, to my sisters and brothers, for always providing me a place I can escape to when everything goes wrong.

Declaration

I certify that this thesis, submitted for the degree of Master of Physics to the department of Physics at Birzeit University, is my own research except where otherwise acknowledged, and that this thesis (or any part of it) has not been submitted for a higher degree to any other university or institution.

Sami Mukhiemer

Signature.....

Contents

List of Figures

List of Tables

Chapter 1

Introduction

1.1 Covariant Density Functional Theory

The atomic nucleus is made up of many nucleons(protons and neutrons), that interact with each other, thus one can treat it as a many body problem.

Density functional theory (DFT) is a tool that was developed by Kohn and Sham, and it was implemented in nuclear structure through the self-consistent mean-field approach [1–4]. Further more, in nuclear physics one can take the interaction between nucleons to be either relativistic or non-relativistic. The relativisitc version of DFT is called covariant density functional theory (CDFT).

K. Karakatsanis et.al [5] applied CDFT to study the structure of the atomic nuclei. Moreover, if one had a full quantum-mechanical nuclear many-body problem, and it was considered as a single-particle problem, then the exact solution of this problem is determined by Slater determinant, and the corresponding single particle density matrix that generated from the product of

single-particle states. By applying a variation principal on the energy functional with respect to this density matrix, so one had the equation of motion of the independent moving nucleons, the specific form of density functional leads to a certain form of the mean field.

If one looked back at the history of DFT in nuclear physics, he could deduce that there were two forms, the most widely known forms are Skerme-type functionals [6] which based on zero-range interactions, and Gogny-type functionals [7] with finite-range interactions. Both models had been successful in describing bulk and structure properties of nuclei along beta stability line giving very similar results [5].

As we said, that nucleus is considered as a many body problem, and one of the of the ways to overcome the hardness of many-body problems is CDFT [8] which is another approach to the non-relativistic methods. CDFT is built on Lorentz covariance and the Dirac equation, it takes the spin degrees of freedom into considerations [9, 10] and it provide an accurate description of spin-orbit splittings [9](see also Fig. 2 in Ref. [11]), also it leads to better understanding of nuclear forces and better description of atomic nuclei [12]. Lorentz covariance of the CDFT equations leads to the fact that time-odd mean fields of this theory are determined as spatial components of Lorentz vectors and therefore coupled with the same constants as the time-like components [13] which are fitted to ground state properties of finite nuclei. In addition, pseudo-spin symmetry finds a natural explanation in the relativistic framework [14].

Over the years many nuclear phenomena have been successfully described within the CDFT [8]. It was successfully described ground state properties of spherical and deformed nuclei [12]. It has been also successful used in the

description of the atomic nuclei behavior in extreme conditions such as high spin and deformation (Super- and hyper-deformation). Super-deformation (SD) was discovered thirty years ago in ^{152}Dy [15]. The tremendous success of (CDFT) was description of fission barriers for many nuclei even if it super heavy nuclei [16]

Hyper-deformation (HD) is another important phenomena in nuclear structure, which will enable us to advance our knowledge of nuclei at extreme conditions of very large deformation and fast rotation. CDFT was very successful in describing and predicating the experimental observation of discrete HD bands, in the Z=40-58 part of the nuclear chart. The spin at which HD bands become yrast was identified, and it was predicted that ^{107}Cd was the best candidate to observe discrete HD bands [17, 18].

G.A. Lalazissis, P. Ring [34], they have shown a calculated results for ground states properties of spherical and deformed nuclei using the CDFT with DD-ME2 as the effective interaction, They calculated the binding energy for approximately 400 nuclei and they compare there results with experimental values, then they concluded that the CDFT with DD-ME2 as the effective interaction was highly successful in describing the ground state properties.

H. Abusara [20], has studied the fission barrier of actinides, and super-heavy nuclei, using CDFT he calculated the fission barrier in axially symmetric relativistic mean field and Bardeen-Cooper-Schrieffer(BCS) approach, and he concluded that the avarge deviation of the hight of the fission barrier is reduced by 30%.

The Walecka model [21] and its extensions with meson carrying isospin [22] are not able to provide quantitative description of nuclei, its compressibil-

ity is two much large and the surface properties are not produced well, in particular deformation are much too small [23]. In order to obtain realistic density functional one needs an additional density dependence [8], over the years three types of models have been developed, non-linear meson coupling models [24–27], density dependent meson coupling models [28–30], and point coupling models with density dependent vertices's.

1.2 Octupole Deformation

The shape of the atomic nuclei in ground state is one of the important properties that we try to study in nuclear structure, the shape of the nucleon is related to interaction between single particle state.

Mottelson [31], showed that breaking of rotational symmetry is spontaneously induced by coupling between individual particle motions and the collective motion. Furthermore interaction between the pairing and spatial deformation, plays an important role in nuclear structure. So one can realized that the deformation is a fundamental element to determine spectroscopic properties of nuclei [32].

S. Ebata, et.al. [32] calculated the ground state deformation of 1002 even-even nuclei, in the mass region with Z=6-92 and $Z \leq N \leq 2Z$. They found that the 58.5% of even-even nuclei are quadrapole deformed. Among them, the ratios of prolate, oblate, and triaxial nuclei are 70%, 12%, and 18% respectively. They also found that octupole deformed nuclei are obtained by a correlations between the shell structure and the pairing correlation, and they concluded that pairing affect the number of even-even octupolly deformed nuclei. In their calculations 30 nuclei were octupolly deformed and

they did not take pairing into account. Most of these nuclei appeared in the nuclear chart which are located in the region of 84<N<88 with 54<Z<70, and 130<N<136 with 84<Z <92.

From a microscopic point of view, symmetry breaking is always associated with pairs of quantum states that are almost have same energy. In quantum systems something like hydridization leads to reduce stability, and even an infinitely small perturbation of a degenerate system produces final response in the system due to rearrangement of many close states. For instance coupling between intrinsic states of opposite parity is produced by long-range octupole-octupole residual interaction. In some cases the mixing is very strong such that a nucleus will possess a stable octupole deformation in the body-fixed frame. For normally deformed systems the condition for octupole coupling occurs for particle numbers associated, with the maximum number $\Delta N = 1$ interaction between the intruder sub shells(l, j) and normal parity sub shells $(l-3, j-3)$ the regions of nuclei with strong octupole correlations corresponding to particle numbers $34(g_{9/2} \longleftrightarrow p_{3/2}$ coupling), $56(h_{1/2} \longleftrightarrow d_{5/2}$ coupling), $88(i_{13/2} \longleftrightarrow g_{9/2}$ coupling) the tendency towards octupole deformation occurs just above closed shells [33]. Single particle states and the number of particles are shown in figure 1.1 [34]. So our region of interest is $(Z \sim 56, N \sim 88)$

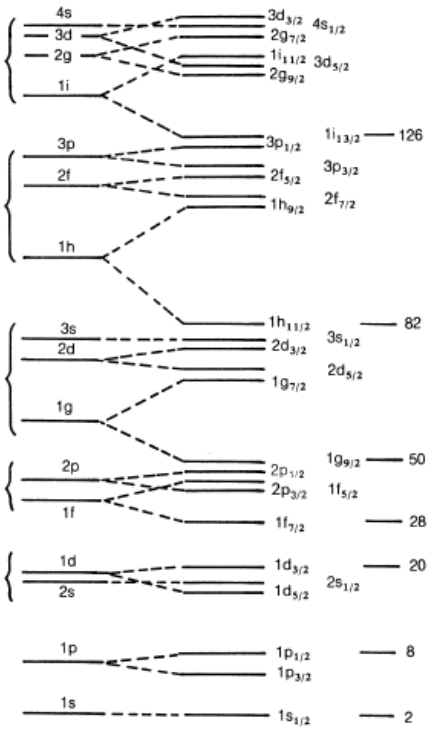

Figure 1.1: Nuclear energy levels in a diffuse potential well. At the left are the levels obtained without spin-orbit coupling and, to the right, the levels obtained with spin-orbit coupling.

The importance of octupole correlation in deformed nuclei has been emphasized over the past 30-40 years. [35–37]

If we can expand the surface radius that defined as:

$$R(\theta,\phi) = R_0[1 + \sum_{lm}[a_{lm}Y_{lm}(\theta,\phi)]] \tag{1.1}$$

Where R_0 is equilibrium radius, a_{lm} is the deformation deviating from spherical shape, and Y_{lm} is the spherical harmonics. One can see the term Y_{30} which represents the octupole shape which is equal:

$$Y_{30} = \frac{1}{4}\sqrt{(\frac{7}{\pi})}(5cos^3(\theta) - 3cos(\theta)) \tag{1.2}$$

An explanation of the behavior of the energies would be an existence of the stable octupole deformation of the nuclei. The potential energy surface as a function of octupole deformation parameter ε_3 (where ε_3 is $a_{30} = \beta_3$) would look them as in figure 1.2. In such case the ground state rotational band $K^\pi = 0^+, I^\pi = 0^+, 2^+, 4^+, ...$ Were the excited rotational band $K^\pi = 0^-, I^\pi = 1^-, 3^-, 5^-, ...$ of even-even nucleus would be displaced by an energy shift ΔE, which is strongly dependent on octupole barrier hight E_B the situation will be similar in Sm isotopes [38].

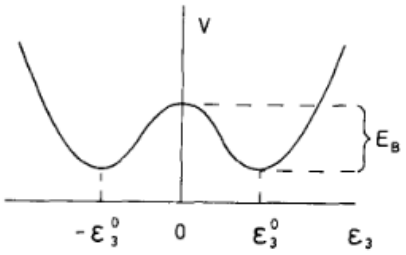

Figure 1.2: Potential energy as a function of octupole deformation parameter

Single-particle spectrum provide an evidence of existence of octupole deformation [31], the reason is that the octupolarity is enhanced when in a given major shell the intruder interacts with standard parity orbital with three unit less of angular momentum. This happens where both protons and neutrons feel strong octupole interaction, octupole-related effects are expected [39].

The field of octupole deformation is the most quickly expanding area of nuclear structure [33], such like the discovery of nuclear quasi-molecular bands, parity doublets and collective intrinsic dipole moments certainly gave the octupole deformation strong push.

This thesis organized as follows: CHAPTER (2) contains formalism of the

general concept of covariant density functional theory, the formalism of the two parameterizations (non linear meson coupling, and density-dependent meson nucleon coupling), and mass moments constraints. In CHAPTER(3) results for potential energy surfaces, and physical properties, was presented, discussed, and compared with other models. In CHAPTER (4) summary and main results was presented, and future work was suggested.

Chapter 2

FORMALISM

2.1 General Concept of Covariant Density Functional Theory

Deformed nuclei were studied by CDFT, and it describe successfully the ground state properties [32]. It follows three assumptions [40]:

1. Nucleons are treated as point-like particles.
2. The theory is fully Lorentz invariant (see 2.1.1)
3. It obeys strictly causality. One can deduce form the previous assumptions that the nucleons is Dirac spinor(ψ).

2.1.1 Mesons

Nucleons are interacting by exchange of particles called Mesons, they distinguished by their quantum numbers(Spin(J), Parity(P), and isospin(T)), their

masses M_m. However the values of their masses, and their coupling constants are fitted to experimental values.

In CDFT nucleons are treated as dirac spinners, and they interact by the exchange of several mesons namely, scalar σ-meson causing medium range interaction, the vector ω-mason leading to strong short range repulsion, and isovector ρ-meson which guaranty that the proton-neutron interaction taking the T= 1, the source of this field are given in the self consistent way by nucleonic and current densities.

1. σ-meson: It has a spin (J)=0, isospin(T)=0, and parity(P)=+1. The corresponding field is $\sigma(x)$.

2. ω-meson: It produce a vector field $\omega^{\mu}(x)$, the time like component is strongly repulsive, in close analogy to coulomb repulsion. The coupling constant $m_{\omega} \approx 738$MeV, the spin of ω=1, P=-1, and the isospin is zero.

3. ρ-meson: Its isospin value T=1, spin(J)=1, and P=-1.

2.1.2 Lagrangian Density

Nucleus composed of fermions , so it act like many body quantum mechanics system, in which those fermion are interacting by the exchange of several mesons, so the classical lagrangian density can be written as:

$$\mathcal{L} = \mathcal{L}_{Nucleon} + \mathcal{L}_{meson} + \mathcal{L}_{int} \tag{2.1}$$

Where $\mathcal{L}_{Nucleon}$ is nucleon Lagrangian density and it given by:

$$\mathcal{L}_{Nucleon} = \bar{\psi}\gamma\left(i\partial - m\right)\psi \tag{2.2}$$

ψ is the Dirac spinor and m is the nucleon mass.

The Lagrangian density of the meson ($\mathcal{L}_{meson}$), and electromagnetic field is

$$\mathcal{L}_{meson} = \frac{1}{2}\partial_\mu\sigma\partial_\mu\sigma - \frac{1}{2}m_\sigma^2\sigma^2 - \frac{1}{4}\Omega_{\mu\nu}\Omega^{\mu\nu} + \frac{1}{2}m_\omega^2\omega^2 - \frac{1}{4}\vec{R}_{\mu\nu}\vec{R}^{\mu\nu} + \frac{1}{2}m_\rho^2\vec{\rho}^2 - \frac{1}{4}F_{\mu\nu}F^{\mu\nu}$$

Where

$$\Omega_{\mu\nu} = \partial_\mu\omega_\nu - \partial_\nu\omega_\mu$$

$$\vec{R}_{\mu\nu} = \partial_\mu\vec{\rho}_\nu - \partial_\nu\vec{\rho}_\mu$$

$$F_{\mu\nu} = \partial_\mu A_\nu - \partial_\nu A_\mu$$

Where A is the vector potential.

The interaction Lagrangian density term is given by:

$$\mathcal{L}_{int} = -\bar{\psi}\left(g_\sigma\sigma + g_\omega\gamma^\mu\omega^\mu + g_\rho\vec{\tau}\gamma^\mu\rho_\mu + e\frac{1-\tau_3}{2}\gamma^\mu A_\mu\right)\psi \tag{2.3}$$

The stationary Dirac equation for nucleon(spinner field) ψ_i (i=1,.....A) in intrinsic frame is given by

$$\hat{h_D}\psi_i = \epsilon_i\psi_i \tag{2.4}$$

Where $\hat{h_D}$ is the Dirac Hamiltonian for a nucleon with mass m

$$\hat{h}_D = \alpha[-i\nabla - V(r)] + V(R)_0 + \beta[m + S(r)] \tag{2.5}$$

The terms shown in the Dirac Hamiltonian are; $V(\vec{r})$, which is the space like component of the potential, and is called the magnetic potential, $V_0(\vec{r})$ is the time like component of potential, which are due to the ω, ρ mesons and the photon, and a scalar field due to the σ-meson. [13]. These terms are writen as follows:

$$V(r) = g_\omega\omega(r) + g_\rho\tau_3\rho(r) + e[\frac{1-\tau_3}{2}]A(r) \tag{2.6}$$

and the repulsive time like component of of the vector field $V_0(r)$

$$V_0(r) = g_\omega \omega_0(r) + g_\rho \tau_3 \rho_0(r) + e[\frac{1-\tau_3}{2}]A_0(r) \tag{2.7}$$

The attractive scalar field S(r).

$$S(r) = g_\sigma \sigma(r) \tag{2.8}$$

Meson fields are described by the Klein-Gordon equations, the corresponding meson field and the electromagnetic potential also determine by this equations, [13, 41]

$$\begin{aligned} \left\{-\bigtriangledown^2 + m_\sigma^2\right\}\sigma(r) &= -g_\sigma[\rho_s^n(r) + \rho_s^p(r)] \\ &\quad -g_2\sigma^2(r) - g_3\sigma^3(r), \end{aligned} \tag{2.9}$$

$$\left\{-\bigtriangledown^2 + m_\omega^2\right\}\omega_0(r) = g_\omega[\rho_v^n(r) + \rho_v^p(r)], \tag{2.10}$$

$$\left\{-\bigtriangledown^2 + m_\rho^2\right\}\rho_0(r) = g_\rho[\rho_v^n(r) - \rho_v^p(r)], \tag{2.11}$$

$$-\bigtriangledown^2 A_0(r) = e\rho_v^p(r), \quad -\bigtriangledown^2 A(r) = ej^p(r), \tag{2.12}$$

The source terms $\rho_s^{n,p}(r)$,and $\rho_\nu^{n,p}(r)$,and involve various nucleic densities currents :

$$\rho_s^{n,p}(r) = \sum_{i=1}^{N,Z}[\psi_i(r)\dagger]\beta\psi_i(r) \tag{2.13}$$

$$\rho_\nu^{n,p}(r) = \sum_{i=1}^{N,Z}[\psi_i(r)\dagger]xs\psi_i(r) \tag{2.14}$$

The n,p in eqs.(2.13, and 2.14) denoted for neutron, and proton respectively, the magnetic potential V(r).

2.1.3 Pairing Correlation

Pairing correlation is important in open shell nuclei, it plays a role for this type of problems, so constant gap of Bardeen-Cooper-Schrieffer(BCS) was

used. The pairing energy expression is written as:

$$E_{pair} = -G[\sum_{i>0} u_i v_i]^2 \tag{2.15}$$

where G is pairing force constant, u_i and v_i are occupation probabilities, and u_i^2=1-v_i^2. [42, 43].

The simple form of BCS equation can be derived from variational method with respect to occupation number v_i^2 and is given by:

$$2\epsilon_i u_i v_i - \triangle(u_i^2 - v_i^2) = 0 \tag{2.16}$$

using

$$\triangle = -G\sum_{i>0} u_i v_i \tag{2.17}$$

The occupation number is defined as

$$n_i = v_i^2 = \frac{1}{2}[1 - \frac{\epsilon_i - \lambda}{\sqrt{(\epsilon_i - \lambda)^2 + \triangle^2}}] \tag{2.18}$$

The chemical potentials λ, are determined by the avarge particle number, and ϵ_i are the eigenvalues of dirac equation. The sum over i in Eqs.2.1.3, 2.17, 2.1.3 run over states in pairing window $E_i < E_{cutoff}$

In Ref. [44] empirical pairing gap parameters have been determined by the systematic fit to experimental data on neutron and proton gaps in the normal deformed minimum.

$$\Delta_p = \frac{4.8}{Z^{1/3}} \tag{2.19}$$

$$\Delta_n = \frac{4.8}{N^{1/3}} \tag{2.20}$$

Where Z is proton number, and N is the number of neutrons.

Shan-Gui Zhou [45] studied the deviation of intrinsic nuclear shapes, he deduced that the intrinsic nuclear shapes deviating from a sphere not only manifest themselves in nuclear collective states but also play important role in determining nuclear potential energy surfaces(PES's), and fission barriers. Pairing is the most striking phenomenon whose description requires an extension of the extreme Mean-Field model [46].

As a results of this importance Chong Qi, and Tao Chen [47], solved analytically the pairing problem and they found an exact solution. They proved that the simple Bardeen-Cooper-Schrieffer(BCS) approximation and generalized Hartree-Fock-Bogoliubov theory(HFB)are successfully describing the pairing properties of open shell nuclei.

In 2017 V.De Donno, and G.Co, M.Anguiano [46] investigated the effect of pairing in spherical nuclei, They used finite range interaction of Gogny type in three steps, Hartree-Fock, Bardeen, Cooper and Schriffe. They concluded that pairing increase the values of excitation energy in all cases. Pairing is known to play an important role in low energy nuclear excitations for the ground state, and it is usually treated within (BCS) or Hartree-Fock-Bogoliubov(HFB) method. [48, 49]

2.2 Parameterizations of the Lagrangian

In this study, we intend to test the sensitivity of our calculations to the choice of parameterization.

For the work in this thesis we choose to perform calculation using meson

exchange models. In this model one can use non-linear model, or density dependent model. The calculation will be done by using both of them, the set NL3* for non-linear model, and DD-ME2 for density dependent model.

As you will see in the next sections, that the two parameterizations are widely used in many nuclear physics applications, for example NL3* was used for fission barrier calculations, and DD-ME2 was used for the physical properties of different types of nuclei(octupolly, and axially deformed nuclei), for instance DD-ME2 was used for finding the mean proton and neutron radii for Ce isotopes.

2.2.1 Non-linear Meson Coupling

A density dependence via a non-linear meson coupling was introduced by Boguta and Bodmer [50], replaced the term $\frac{1}{2}m_\sigma^2\sigma^2$ in equation 2.3 with

$$U(\sigma) = \frac{1}{2}m_\sigma^2\sigma^2 + \frac{1}{3}g_2\sigma^3 + \frac{1}{4}g_3\sigma^4 \tag{2.21}$$

Where m, m_σ, and m_ρ are fixed values of masses, and there is six phenomenological parameters (m_σ, g_σ, g_ω, g_ρ, g_2, g_3) as shown in table 2.1.

Table 2.1: NL3* and DD-ME2 parameterizations of the RMF Lagrangian

parameter	NL3*	DD-ME2
m	939	939
m_σ	502.5742	550.1238
m_ω	782.600	783.000
m_ρ	763.000	763.000
g_σ	10.0994	10.5396
g_ω	12.8065	13.0189
g_ρ	4.5748	3.6836
g_2	-10.8093	0.0000
g_3	-30.1486	0.0000
a_σ	0.0000	1.3881
b_σ	0.00000	1.0943
c_σ	0.0000	1.7057
d_σ	0.0000	0.4421
a_ω	0.0000	1.3892
b_ω	0.0000	0.9240
c_ω	0.0000	1.4620
d_ω	0.0000	0.4775
a_ρ	0.0000	0.5647

In 2009,G. A. Lalazissis, S. Karatzikos, et.al [51] introduced effective force to NL3*, which improved the description of nuclear masses, provided an excellent results for collective properties of vibrational and rotational character.

2.2.2 Density-dependent meson-nucleon coupling

In density dependent meson-nucleon coupling there are no nonlinear terms in the σ meson ($g_2 = g_3 = 0$) The meson-nucleon vertices's are defined as:

$$g_i(\rho) = g_i(\rho_{sat}) f_i(x) \tag{2.22}$$

where $i = \sigma, \omega$, and ρ and.
for σ and ω

$$f_i(x) = a_i \frac{1 + b_i(x + d_i)^2}{1 + c_i(x + d_i)^2} \tag{2.23}$$

But for ρ

$$f_\rho(x) = \exp(-a_\rho(x - 1)) \tag{2.24}$$

Where x is defined as the ratio between the baryonic density ρ at a specific location and the baryonic density at saturation ρ_{sat}. one can get the values of the parameter form table 2.1. The parameters in equation 2.23 are not independent, but constrained as $f_i(1) = 1, f''_\sigma(1) = f''_\omega(1) = f''(0) = 0$, These constrained reduce the the number of independent parameters for density dependance to three.

In 2005, G. A. Lalazissis, et.al [53], showed that the result for calculated properties of spherical and deformed nuclei using the effective interaction DD-ME2. Pairing correlation have been included in(RHB) model with finite range forces of Gogny. They calculated the binding energy for approximatly 400 nuclei, then compare their results with experimental ones, finally they concluded that there was a vary good agreement between the calculated and the experimental results.

2.3 Quadratic Constraints

The method of quadratic constraints uses an unrestricted variation of the function

$$< H' >= \langle H \rangle + \sum_{\nu=2,3} C_{\nu 0}(\langle \hat{Q_{\nu 0}} \rangle - q_{\nu 0})^2 \tag{2.25}$$

Where $\langle H \rangle$ is the expectation value of Hamiltonian (total energy), $q_{\nu 0}$ is the constrained value of multipole moment, and $C_{\nu 0}$ is the corresponding stiffness constant [48]. Moreover, the quadratic constraint adds an extra force term $\sum_{\nu=2,3} \lambda_\nu \hat{Q}_{\nu 0}$ to the system, where

$$\lambda_\nu = 2C_{\nu 0}(\langle \hat{Q_{\nu 0}} \rangle - q_{\nu 0})^2 \tag{2.26}$$

For a self consistent solution. This term is necessary to force the system to a point in deformation space different from a stationary point. The augmented Lagrangian method [54] has also been implemented in order to resolve the problem of convergence of the self-consistent procedure which diverges while increasing the value of stiffness constant.

And $\langle \hat{Q_{\nu 0}} \rangle$ denotes the expectation value of mass quadrapole and octupole operators. The quadrapole and octupole moment constraint can applied with the following relations:

$$< \hat{Q_{20}} >=< \hat{Q_{20}} >_n + < \hat{Q_{20}} >_p \tag{2.27}$$

$$< \hat{Q_{30}} >=< \hat{Q_{30}} >_n + < \hat{Q_{30}} >_p \tag{2.28}$$

The deformation parameter β_2 and β_3 are related to $< \hat{Q_{20}} >$ and $< \hat{Q_{30}} >$

by the following relation

$$< \hat{Q_{20}} >= \frac{3}{\sqrt{5\pi}} A r^2 \beta_2 \tag{2.29}$$

$$< \hat{Q_{30}} >= \frac{3}{\sqrt{7\pi}} A r^3 \beta_3 \tag{2.30}$$

Where $r = R_0 A^{\frac{1}{3}}$, $R_0 = 1.2fm$, and $A(A = Z + N)$ is the nucleon number.

By constraining quadrapole moment and octupole moment simultaneously the total energy surface in the (β_2, β_3) plane can be obtained.

Chapter 3

Discussion of Results

We perform a systematic calculations along the Sm isotopic chain, mapping the potential energy surface for all even-even nuclei, to determine the effect of octupole deformation. In this chapter results for both parameterizations NL3*, and DD-ME2 will be discussed. Then we compare the binding energies, two neutron separation energy, neutron and proton radii, and the location of global minimums for each parametrization.

3.1 Potential Energy Surfaces

We perform constrained calculation on quadratic and octupole mass moments and plot the binding energy as a function of β_2, and β_3.

Figures [3.1-3.3] display potential energy surfaces (PES) in β_2-β_3 plane calculated using constrained covariant density functional theory (CDFT)with non-linear model using the parameter set NL3* for even-even Sm isotopes with mass number 140-160.

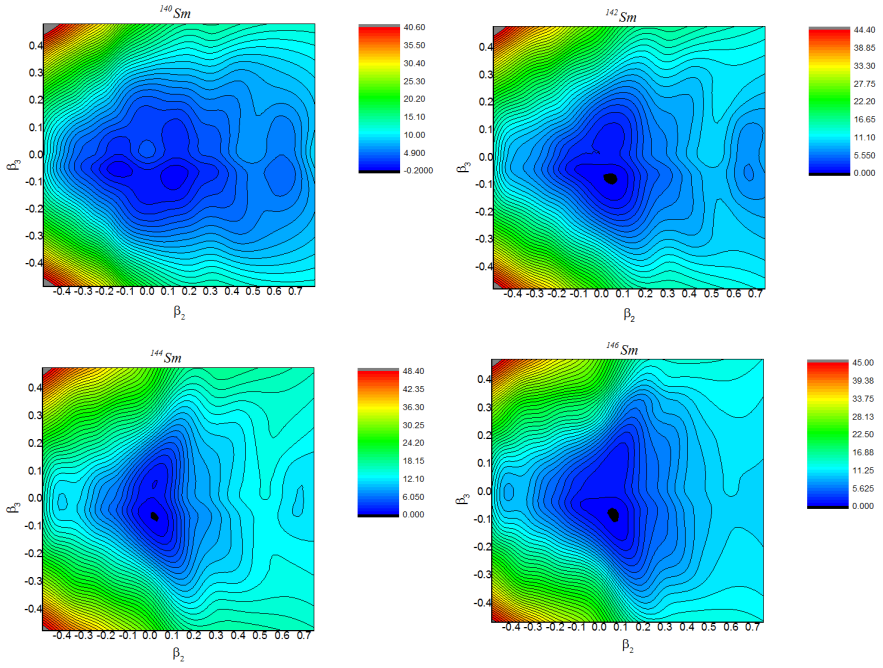

Figure 3.1: Potential energy surface for ^{140}Sm, ^{142}Sm, ^{144}Sm, and ^{146}Sm in β_2 and β_3 deformation space using NL3* parametrization.

In upper left panel of figure 3.1, for ^{140}Sm we can see the existence of two local minimums, one of them is located near β_3 =0 and β_2 = -0.20, while the other one is near β_2 = 0.15. The difference in energy between these two minimum is around 3.4 MeV. However, near the deepest minimum one can see that the ground state extend from β_3 = 0 to β_3 -0.2. Thus there exist a possibility of octupolly deformed ground state. And the binding energy per nucleon(As seen in next section was approx. -8.25). Similar behavior can also be seen in the case of ^{142}Sm, shown in upper right of figure 3.1 but with a decrease in the energy difference between the two minimum to around 3 MeV as listed in table 3.1. And the minimums was less octupolly deformed so we expect that the nuclei will be more stable than ^{140}Sm.

As we move along the isotopic chain to ^{144}Sm one can notice that the ground state island located at (β_2) form ≈ -0.1 to ≈ 0.1, which can be seen in down left of figure 3.1, and the island started to extend in the direction of β_3 away from β_3 =0, and cover the range from -0.15 up to 0.15. So the minimum island of ^{144}Sm is not octupolly deformed so it has the largest binding energy per nucleon(The most stable nuclei in the chain). Thus we can see that indeed the octupole deformation starts to play a role in defining the ground state properties.

For ^{146}Sm, the down right panel of figure 3.1 shows that the value of β_3 increases up to 0.2. This increase made the binding energy per nucleon decrease so as the value of octupole deformation increased the binding energy per nucleon decrease. The ground state island is located between 0.1 to -0.1 in the β_2 direction. This is similar to result of ^{144}Sm. One can notice a smooth change in the PES along the isotopic chain, that is the transition from a specific nuclear shape to another one through the chain is not sudden. The connection of this smooth transition to other physical observables such as binding energy, binding energy per nucleon, two neutron separation energy, proton and neutron radii, will be discussed later in this chapter.

The case of ^{148}Sm, shown in upper left panel of figure 3.2, is very interesting one, as we can clearly see the development of two distinct minimum. The first one is axially deformed(oblate)with no octupole deformation, and the second one is an island that is elongated along the β_3 direction and ranging from -0.25 to 0.25, and at $\beta_2 = 0.2$. As a results of that we see a decrease in the binding energy per nucleon. This island has some kind of necking around β_3, thus we might expect that as we increase the number of neutrons to see this island split into two distinct parts.

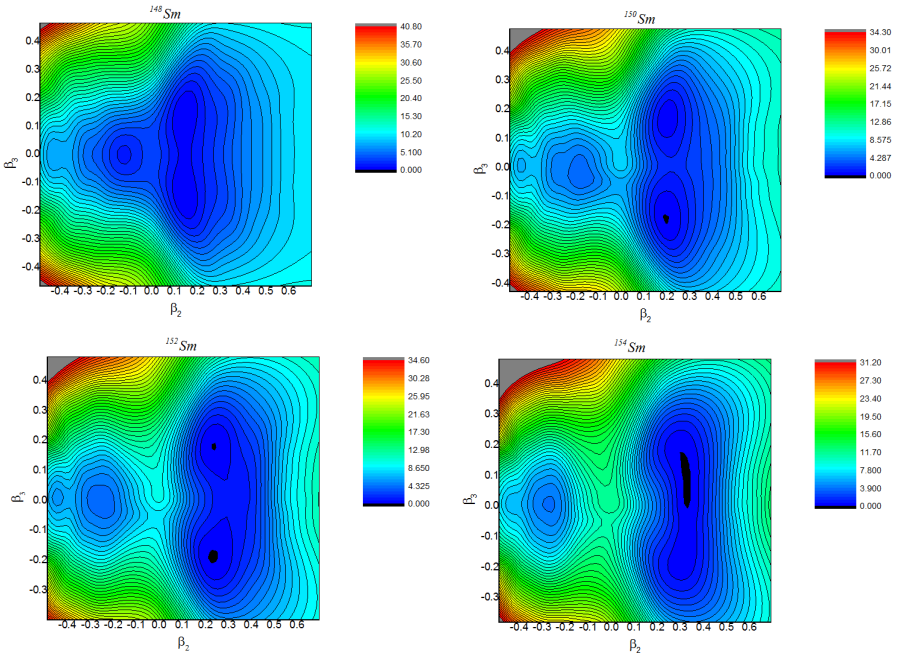

Figure 3.2: Potential energy surface for ^{148}Sm, ^{150}Sm, ^{152}Sm,and ^{154}Sm in β_2 and β_3 deformation space using NL3* parametrization.

In upper right panel of figure 3.2 does indeed shows that there is two distinct minimum for ^{150}Sm, located at β_2 =0.20 and $\beta_3 = \pm 0.2$. In addition to that there is another minimum, not octupole deformed, that is higher in energy located at β_2 = -0.2. Similar trend continues to show up in the case of ^{152,154}Sm, seen in down panel of figure 3.2, but in ^{154}Sm one of the minimums located at $\beta_3 = 0.15$ and $\beta_2 = 0.30$., the other one, centered at $\beta_3 = 0$ and β_2 =-0.2. and there is a barrier with 14MeV potential separate the two minimums, the energy difference between the two minimums 4MeV. Not like other Sm isotopes there is a symmetry in energy values around $\beta_3 = 0$. As one could notice also form figure 3.2 as the β_3 increase, the stability of nuclei will decrease.

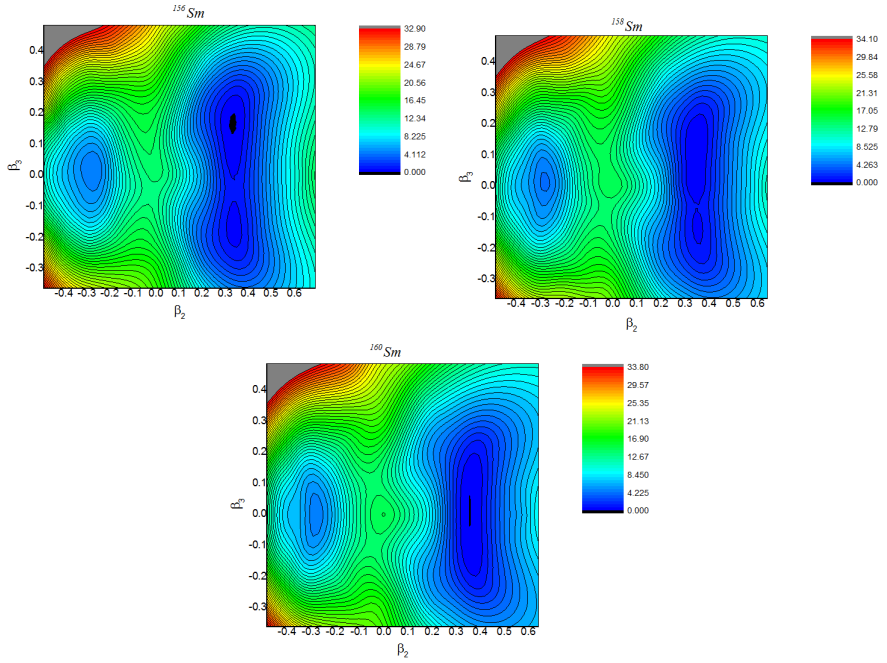

Figure 3.3: Potential energy surface for ^{156}Sm, ^{158}Sm,and ^{160}Sm in β_2 and β_3 deformation space using NL3* parametrization

In upper right panel of figure 3.3, there exist a barrier between the two minimums for ^{156}Sm of width(16MeV), and also the energy difference between the two minimum islands was 6 MeV which is larger than the one seen in ^{154}Sm. One of those minimum is located at $\beta_3 = 0.15$ and $\beta_2 = 0.30$, and the second one is located at $\beta_3 = 0$ and β_2 = -0.25. Similar to the cases of ^{150}Sm, ^{152}Sm and ^{154}Sm one of the minimum is octupoly deformed and the other one is not. In upper right and down panels of figure 3.3, where ^{158}Sm, and ^{160}Sm are shown respectively. They have the same pattern as ^{156}Sm, where the barrier between the two minimums, and the energy difference between them has increased. The following table summarizes the location of the two minimums (if exists) in (β_2,β_3) planes and the energy difference between them.

Table 3.1: List of minimums (β_2, β_3) for Sm isotopes and its locations using NL3* parametrization. The first minimum is the deepest one.

Isotope	1^{st} minimum	2^{nd} minimum	ΔE
^{140}Sm	(-0.2,0)	(0.15,0)	3.482640 MeV
^{142}Sm	(0.65,-0.05)	(0.2,0)	2.996795 MeV
^{144}Sm	(0,-0.05)	-	It has one minimum
^{146}Sm	(0.05,-0.10)	-	It has one minimum
^{148}Sm	(-0.10,0)	(0.15,0.05)	1.080943 MeV
^{150}Sm	(-0.15,0)	(0.20,0.20)	3.442387 MeV
^{152}Sm	(-0.25,0)	(0.25,0.20)	3.896257 MeV
^{154}Sm	(-0.25,0)	(0.30,0.15)	3.782354 MeV
^{156}Sm	(-0.25,0)	(0.35,0.15)	4.195289 MeV
^{158}Sm	(-0.30,0)	(0.35,0.15)	4.028288 MeV
^{160}Sm	(-0.30,0)	(0.35,0)	4.439858 MeV

Figures[3.4-3.6] show PES in (β_2, β_3) plane using density dependent meson interaction represented by the parametrizations set DD-ME2 for even-even nuclei with mass number 140-160.

If one compares the upper left panel of figure 3.4, and the upper left panel of figure 3.1, where PES for ^{140}Sm is plotted, two things can be noticed. The first one, that there is a slightly difference in the location of the two local minimums, and the second one also that the shape of the two islands is different. If one refer to table 3.1 and table 3.2 could see that the energy difference between the two minimums are slightly different in two parametrization. As we move forward to upper right panel of figure 3.4, PES of ^{142}Sm, the same pattern to the previous upper left panel of figure 3.4 can be seen. However, there is a decrease in energy difference between the two local minimum as listed in table 3.2. In comparison with the NL3* results, one can notice a difference in the shape of the ground state, but if one look at the stability the binding energy per nucleon were almost the same of NL3* parameterization(see figure 3.7).

As we move forwarded through the chain to ^{144}Sm, shown in down left panel of figure 3.4 it has one global minimum, which is located at (β_2)form$\approx$ 0 to $\approx$ 0.1, and (β_3)form ≈ -0.15 away to $\approx$ 0.15. As a results of circular ground state island, this nuclei is the most stable nuclei in the chain. Thus the octupole deformation plays as important role in defining the ground state properties for this nuclei. If one refer to the down left panel of figure 3.1 there is a difference in the ground state shape between the two parameterizations. In down left panel of figure 3.4 the ground state for ^{144}Sm for has one global minimum, and ^{146}Sm shows a similar pattern. As the value of β_3 increased

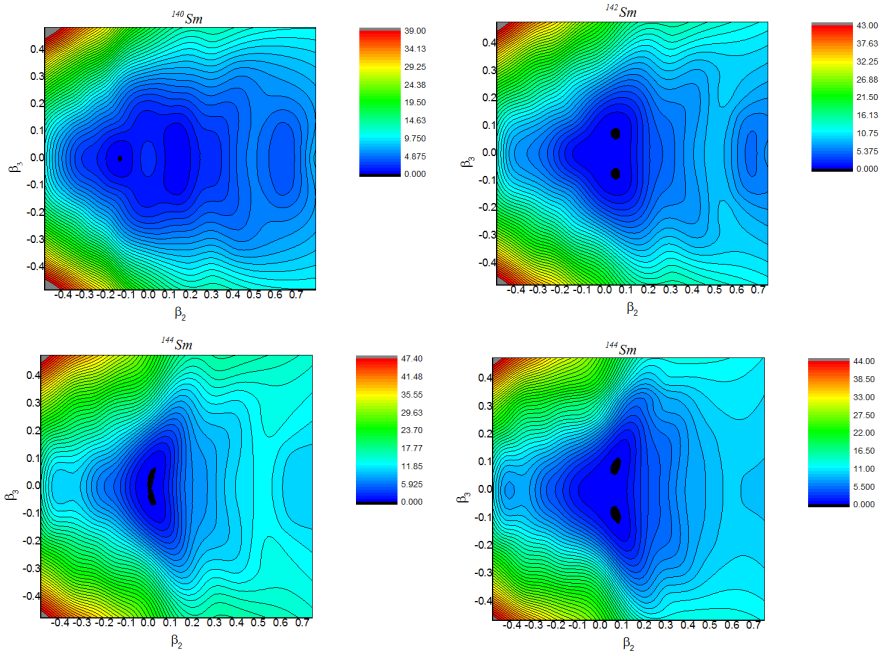

Figure 3.4: Potential energy surface for ^{140}Sm, ^{142}Sm, ^{144}Sm, and ^{146}Sm in β_2 and β_3 deformation space using DD-ME2 parametrization.

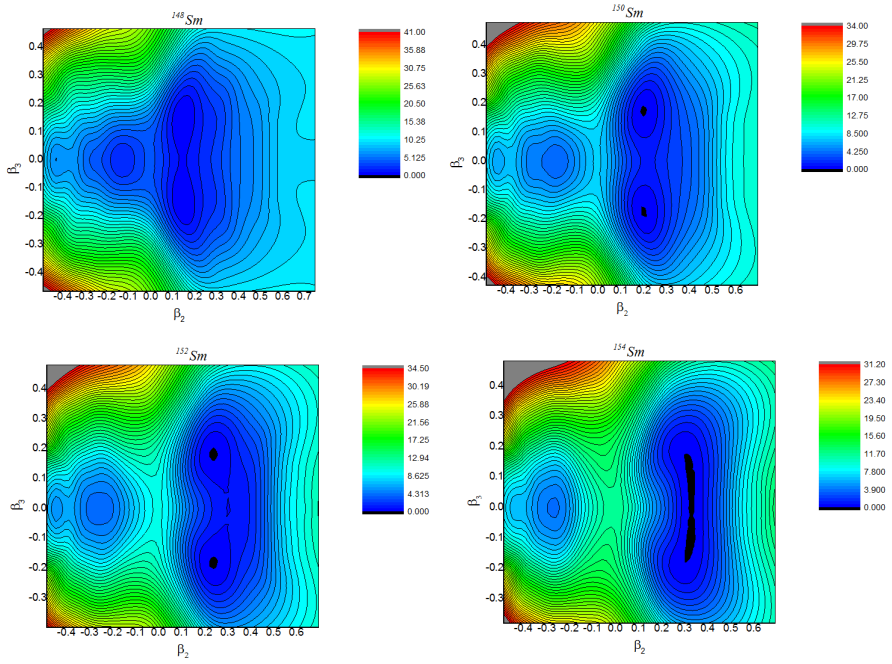

Figure 3.5: Potential energy surface for ^{148}Sm, ^{150}Sm, ^{152}Sm, and ^{154}Sm in β_2 and β_3 deformation space using DD-ME2 parametrization.

the nuclei was less stable.

The case of ^{148}Sm is shown in the upper left panel of figure 3.5, as we can see that we have two distinct minimums developed. Similar to the results obtained with NL3* parametrization, shown in the upper left panel of figure 3.2. One of those minimum has an oblate shape with no octupole deformation, β_2 values ranges from ≈ 0.12 to ≈ 0.20. The second one was directed in β_3 axis, it located at β_2 from ≈ -0.15 to ≈ -0.5.

If one refer to upper left panel of figure 3.2,^{148}Sm with NL3*, there is no significant difference in the shape of the two islands, and one could clearly see that energy difference between the minimum was almost the same in both parametrizations, as can be seen in the two tables 3.2, and 3.1.

The upper right panel of figure 3.5 and the upper right panel of figure 3.2 have similar trends, shows PES for ^{150}Sm. Both of them show two distinct minimums, the first one has an octupole shape elongated at(β_2) form $\approx$ 0.19 to$\approx$ 0.25, and the other one was not octupolly deformed with β_2 form $\approx$ -0.25 to$\approx$ 0.10, the second island has higher energy as shown in table 3.2. One can notice that there is a barrier between the two minimums with energy around 10 MeVs, which did not existed in the down left panel of figure 3.2.

As we move through the chain to ^{152}Sm the same trend was noticed but with increase in potential barrier as obviously appeared in down left of figure 3.5, and if we refer to table 3.2 we can see the increases in the energy difference between the two minimum islands.

In down left panel figure 3.5, ^{152}Sm, one of the minimum located at $\beta_3 = 0.15$ and $\beta_2 = 0.30$, the second one located at $\beta_3 = 0$ and β_2 = -0.25 as appeared in table 3.2. The barrier between the two islands was grater than down right of figure 3.5,^{154}Sm, similar trend appeared in ^{156}Sm but the location of the minimum as appeared in upper left of figure 3.6, and table 3.2 that $\beta_3 = 0.15$ and $\beta_2 = 0.35$,and the second one was $\beta_3 = 0$, and β_2 = -0.25. The energy difference as $\approx 4MeV$.

Both ^{158,160}Sm have the same pattern as clearly seen in figure 3.6, the energy difference between the two minimums was increased and the barrier energy was increased too the following table 3.2 sum up the location of the two minimums(if exists) and also, the energy difference between them.

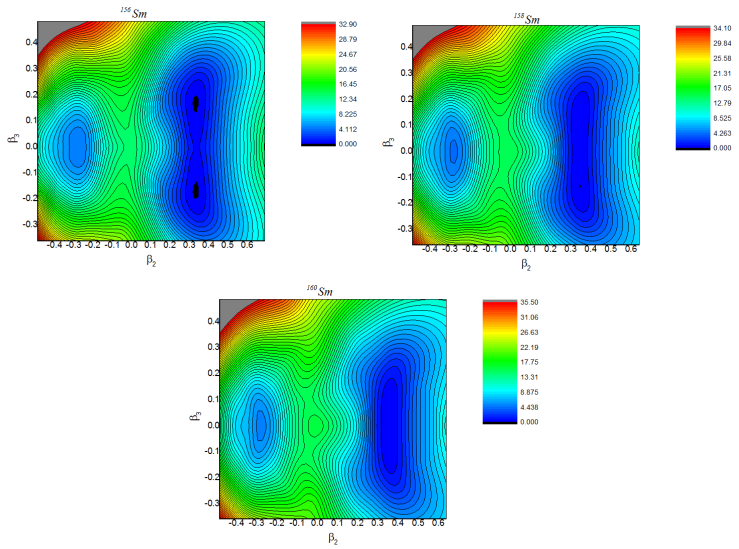

Figure 3.6: Potential energy surface for ^{156}Sm, ^{158}Sm, and ^{160}Sm in β_2 and β_3 deformation space using DD-ME2 parametrization.

Table 3.2: List of global minimums (β_2, β_3) for Sm isotopes and its locations using DD-ME2 parametrization. The first minimum is the deepest

Isotope	1^{st} minimum	2^{nd} minimum	ΔE
^{140}Sm	(0.15,0)	(-0.20,0)	3.422080 MeV
^{142}Sm	(0.65,0)	(0.05,0.05)	5.163854 MeV
^{144}Sm	(0,0)	-	It has one minimum
^{146}Sm	(0.10,0.10)	-	It has one minimum
^{148}Sm	(-0.15,0)	(0.15,0.15)	1.810199 MeV
^{150}Sm	(-0.20,0)	(0.20,0.15)	3.624392 MeV
^{152}Sm	(-0.25,0)	(0.25,0.15)	3.903804 MeV
^{154}Sm	(-0.25,0)	(0.30,0.15)	3.828174 MeV
^{156}Sm	(-0.25,0)	(0.35,0.15)	4.176513 MeV
^{158}Sm	(-0.30,0.05)	(0.35,0.10)	4.263953 MeV
^{160}Sm	(-0.30,0)	(0.35,0)	4.835485 MeV

3.2 Physical Properties

3.2.1 Binding Energy and Two Neutron-Separation Energy

The energy required to disassemble the nucleus into its parts (protons, and neutrons) called the binding energy of nucleus, this energy are due to attractive force between protons and neutrons.

Because of the linearity of the binding energy with nucleon number, it is meaningful to define binding energy per nucleon (E_B/A). The lesser B_E/A less stable nuclei, because lesser binding energy per nucleon are easier to separate the nucleus into its constituent nucleons.

In figure 3.7, the binding energy per nucleon for the two parameterizations (NL3*, and DD-ME2) is shown as and compared with experimental data (see [55]). The sharpness on the curve is due to the increase of the nucleon number.

As one could see from the previous figure 3.7, the two parameterizations agreed with the experimental data that ^{144}Sm are the most stable nuclei in the chain because it has the largest binding energy per nucleon, and ^{160}Sm is the most unstable nuclei in the chain. There were another agreement in the figure between calculated binding energy by both parameterizations (NL3*, and DD-ME2), and the experimental one, this agreement was for ^{142}Sm, and also one could notice that the binding energy calculated by DD-ME2 parameterizations and the experimental value for ^{150}Sm are almost the same. If one look back to the PES's he could deduce that there is a

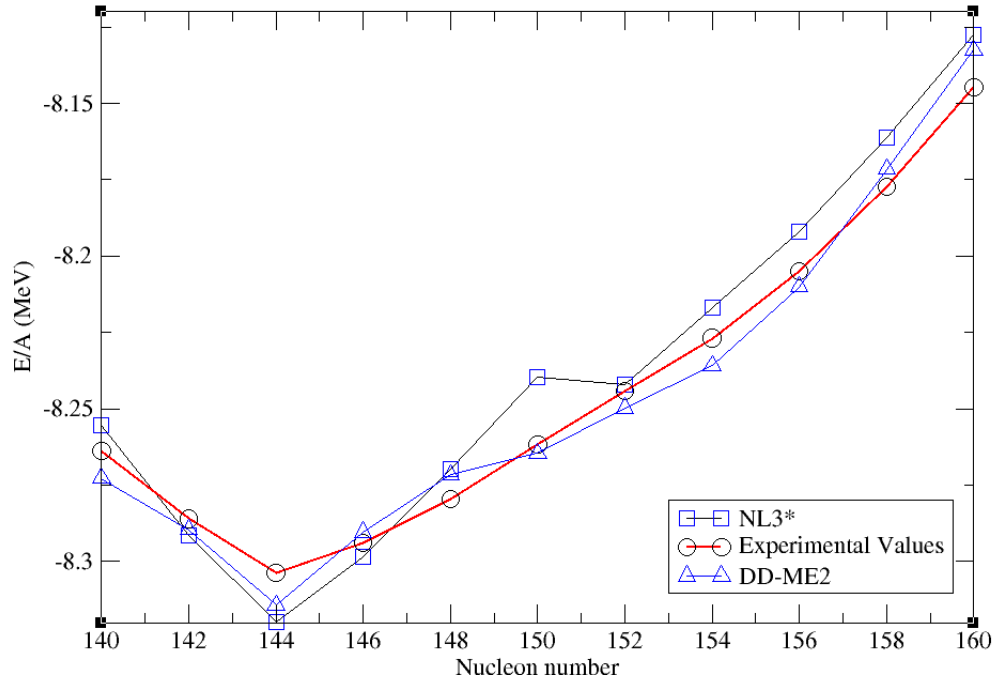

Figure 3.7: Binding energy per nucleon using NL3*,DD-ME2, and experimental data

relationship between octupole deformation and stability, as we saw before ^{144}Sm was the most stable nuclei in the chain and it has the smallest octupolly deformed ground state island(see figures 3.1, and 3.4), were ^{160}Sm has the largest octupully deformed ground state islands as a results it has the smallest binding energy per nucleon(see figures 3.3, and 3.6).

In the following figure 3.8 we analyze the behavior of two neutron separation energy, which is defined as follows:

$$S_{2n} = BE(N+2, Z) - BE(N, Z) \tag{3.1}$$

Two neutron separation energy is an important quantity used as an indication of nuclear shell closure. We calculate the S_{2n} using two different parameter

sets and compare their results with the available experimental data [56].

As one can deduce form the following figure, there were a very good agreement between the results obtained with CDFT, and experimental data. The sharpness of ^{144}Sm in both figures (3.7, and 3.8) is due to the shell closure at $N = 82$ where 82 is a magic number.

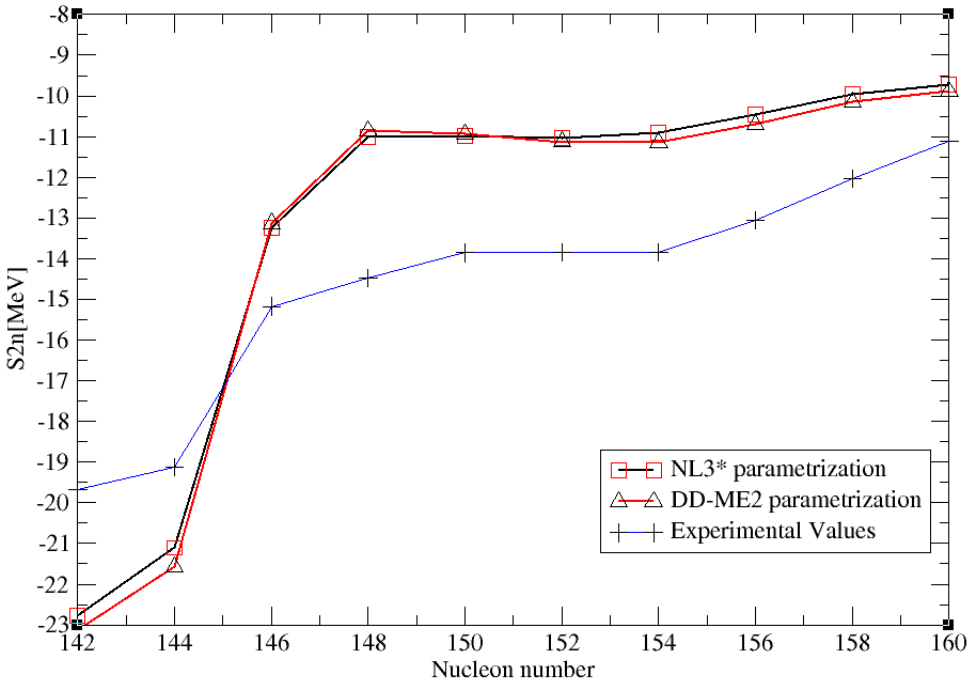

Figure 3.8: Two Neutron-Separation Energy by using NL3*, and DD-ME2 parameterizations in comparison with experimental values

3.2.2 Proton and Neutron Radii

Both parameterizations(DD-ME2, and NL3*) were used to calculate the mean radius of neutron, and proton for even-even Sm isotopes. As obvi-

ously appeared from Fig. 3.9 ^{142}Sm has the smallest mean proton radius and after, as the nucleon number increased the mean proton radius increased as shown in Fig. 3.9 thus protons in ^{160}Sm have the largest mean radii in the chain.

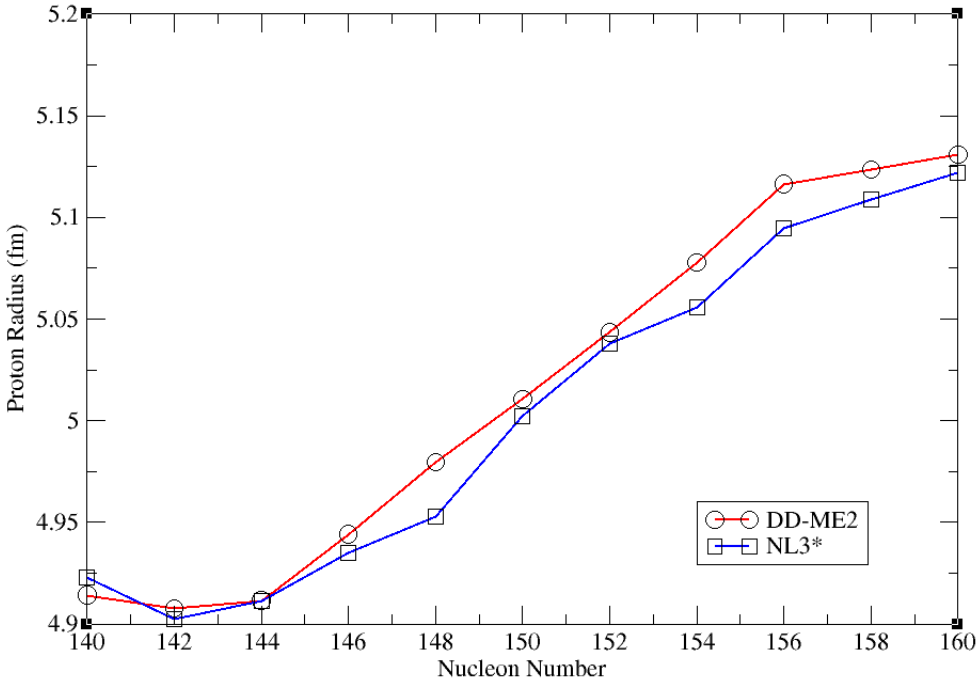

Figure 3.9: Proton mean radius using NL3*, and DD-ME2

As one can noticed from the figures (3.10, 3.9) ^{142}Sm as the smallest mean proton, and mean neutron radii, were ^{160}Sm has the largest proton, and neutron radii. If one compare the results between DD-ME2, and NL3* parameterizations he could conclude that there is an agreement between them. The results by both parameterizations was so close.

As clearly appeared in figure 3.10. If one compare the results with experimental data ([56, 58]), one could see that that the results for DD-ME2 have a better agreement than compared with NL3 *. ^{142}Sm has the smallest radii

in the chain, and the ^{160}Sm has the largest mean neutron radii.

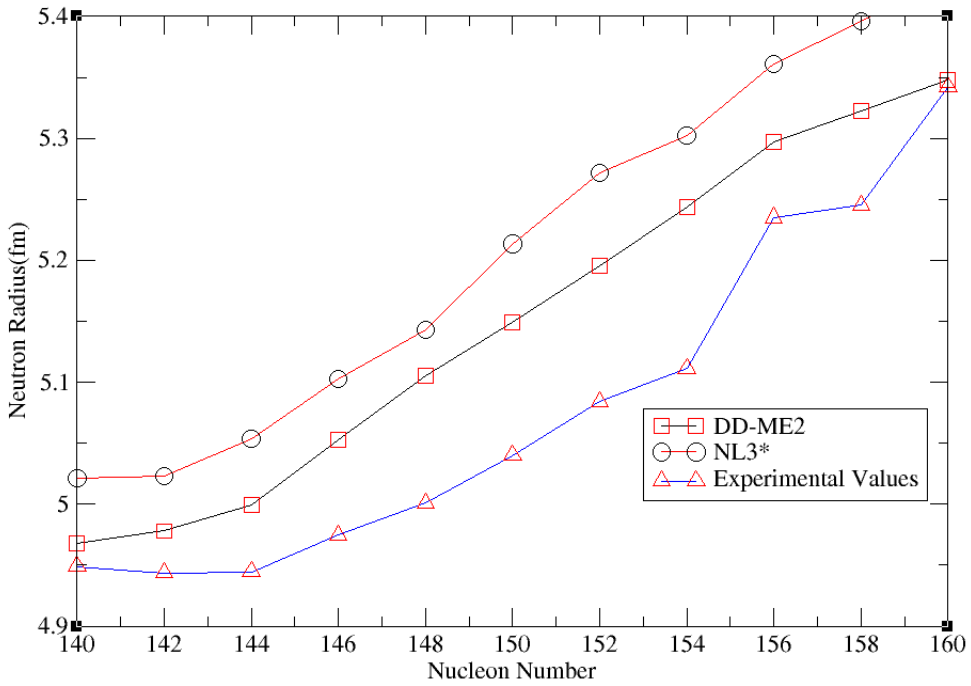

Figure 3.10: Neutron mean radius using NL3*, and DD-ME2, and experimental data [56, 58]

3.3 Comparison with other models

K. Nomara, and D. Vretenar [59] plotted the PESs for $^{146-156}Sm$ in (β_2, β_3) plane, by mapping the deformation constrained self-consistent axially symmetric mean-filed energy onto equivalent Hamiltonian of the sfd interacting boson model (IBM), that based on the gobal relativistic energy density functional(DD-PC1), the ranges of β_3, and β_2 respectively was $0 \leq \beta_3 \leq 0.15$, and $-0.3 \leq \beta_2 \leq 0.5$, because of the symmetry around $\beta_3 = 0$ axis they did not look at the negative values of β_3. They plotted the PESs for Sm

isotopes($^{146-156}Sm$). If one refer to [59] he could deduce the global minimums for Sm isotopes and its locations using interaction boson model(IBM), and DD-PC1 the results was as the following respectively:

Table 3.3: List of minimums for Sm(^{146}Sm-^{156}Sm) isotopes and its locations using IBM model see [59]

Isotope	1^{st} minimum	2^{nd} minimum
^{146}Sm	(-0.05,0)	(0.09,0)
^{148}Sm	(-0.10,0)	(0.15,0)
^{150}Sm	(-0.15,0)	(0.22,0.12)
^{152}Sm	(-0.20,0)	(0.30,0)
^{154}Sm	(-0.25,0)	(0.35,0)
^{156}Sm	(-0.25,0)	(0.35,0.08)

Table 3.4: List of minimums for Sm(^{146}Sm-^{156}Sm) isotopes and its locations using DD-PC1 model see [59]

Isotope	1^{st} minimum	2^{nd} minimum
^{146}Sm	(0.05,0)	-
^{148}Sm	(-0.15,0)	(0.15,0.1)
^{150}Sm	(-0.15,0)	(0.20,0.15)
^{152}Sm	(0,0)	(0.30,0)
^{154}Sm	(-0.25,0)	(0.35,0)
^{156}Sm	(-0.25,0)	(0.35,0.10)

At first if one refer to the tables(3.3,and 3.4) he could deduce that ^{146}Sm has two local minimums as appeared in the IBM results, but in comparison with

our results, both parameterizations(NL3*, and DD-ME2) agreed that it has one Local minimum. The location of the first minimum was far from our results that we found by NL3* and DD-ME2 parameterizations. If one go through the PES's of ^{148}Sm and compare the results of IBM, and DD-PC1 with DD-ME2, and NL3* he could conclude that DD-ME2 results was almost the same of DD-PC1, and the location of the first minimum in IBM was the same of NL3* parameterization but the second minimum was not.

If we moved forward in the chain to ^{150}Sm, we could conclude that the location of the first minimum found by DD-ME2, NL3*, IBM, and DD-PC1 was exactly the same, but there were an agreement in location of the second minimum between DD-ME2 and DD-PC1. Otherwise there were no agreement between IBM, and DD-PC1.

In ^{152}Sm, ^{154}Sm, and ^{156}Sm the location of the first minimum in IBM, DD-PC1, DD-ME2, and NL3* was exactly the same, but the location of the second minimum was almost the same.

W. Zhang, Z. P. Li [60] they calculated the PES's of even- even nuclei $^{146-156}$Sm in (β_2, β_3) plane, that were investigated in the constrained reflection asymmetric-relativistic mean field approach (RAS-RMF) with PK1 as a parameter set, they plotted the contour plots for the total energy in (β_2, β_3) plane that obtained in the RAS-RMF approach with PK1 and constant-Δ paring, and the results were in the following table

Table 3.5: List of minimums for Sm(^{146}Sm-^{156}Sm) isotopes and its locations using RAS-RMF approach with PK1 and constant-Δ paring [60]

Isotope	1^{st} minimum	2^{nd} minimum
^{146}Sm	(-0.10,0)	-
^{148}Sm	(-0.15,0)	(0.15,0.15)
^{150}Sm	(-0.20,0)	(0.20,0.20)
^{152}Sm	(-0.25,0)	(0.20,0.15)
^{154}Sm	(-0.25,0)	(0.30,0.1)
^{156}Sm	(-0.25,0)	(0.35,0)

As one can deduce from the previous table 3.5 and compare the results, with NL3*, and DD-ME2 parameterizations results, he could conclude that the location of the local minimum of^{146}Sm had no agreement with DD-ME2, and NL3*, but if one go through the results of the Sm isotopic chain such like the locations of the local minimums of ^{148}Sm, and ^{152}Sm he could see that the results was the same as DD-ME2 results, the location of the other minimums in the chain such as the local minimums of ^{154}Sm, and ^{156}Sm was almost the same of DD-ME2 results.

Y. El Bassem, M. Oulne, [61] used finite range droplet model(FRDM), and relativistic mean field(RMF) theory to calculate the physical properties for Sm isotopes such like proton radii, neutron radii, binding energy per nucleon, two neutron separation energy for Sm, Nd, and Ce isotopes, and the results were compared with CDFT model, if one took the results of mean proton, and neutron radii for Sm isotopes that calculated by FRDM and RMF in considerations, he could deduced two things, the first one results were so close to the results in figures (3.9, 3.10). The second thing he could conclude that

^{142}Sm has the smallest mean proton, and neutron radii in all models(FRDM, RMF, CDFT).

If one refer to the ref. [61] he conclude that ^{144}Sm is the most stable nuclei in the chain such as CDFT predicted, and also one could see that DD-ME2 results(3.7) was close to the results in [61].

In ref. [61] two neutron separation energy was plotted and compared with FRDM, and RMF models. If one compare the results with our results that plotted by NL3*, and DD-ME2 parameterizations he could see the agreement between the results.

Chapter 4

Conclusion

The ground state properties of even-even Sm isotopes were studied using covariant density functional theory(CDFT), using nonl-linear meson interaction, represented by the set NL3*, and density-dependent meson interaction represented by the set DD-ME2. We mapped the potential energy surfaces defined by octupole and quadrupole deformation. The results of the study can be summarized as follows:

1. The first and second minimum are defined by the octupole deformations, In the majority of the cases. However, the second one is usually soft(flat inβ_3 direction)in the octupole deformation.

2. The results of the study showed that the results of covariant density functional theory is independent of the choice of parametrizations.

3. Potential energy surfaces shows a softness in the direction of β_3 in the first minimum. However, this minimum starts to split into two separate minimum as the nucleon number increases.

4. When the number of nucleon was 150 a barrier between the two min-

imums islands starts to develop to separate the ground state island. Then the barrier width increased as the number of nucleon increased beyond 150 and separate the island.

5. The nucleon mean radius is usually increasing as a function of mass number (A), the results is not sensitive to the choice of parametrization. However, the proton radius is smallest for ^{142}Sm and the neutron radius is smallest for ^{140}Sm

6. Our results is in agreement with the results obtained from other models and experimental data.

Bibliography

[1] P. Hohenberg, and W. Kohn, Phys. Rev. **B 864**, 136 (1964).

[2] W. Kohn, and L. J. Sham, Phys. Rev. **A 1133**, 140 (1965).

[3] W. Kohn, Rev. Mod. Phys. 71, 1253 (1999).

[4] R. M. Dreizler, and E. K. U. Gross, Density Functional Theory, Springer-Verlag, Berlin, 1990.

[5] Konstantinos Karakatsanis, G. A. Lalazissis, Peter Ring, and Elena Litvinova, Phys.Rev. **C 95**, 034318 (2017)

[6] D. Vautherin, and D. M. Brink, Phys. Rev. **C 5**, 626 (1972)

[7] J. Dechargé, and D. Gogny, Phys. Rev. **C 21**, 1568 (1980)

[8] D. Vretenar, A. V. Afanasjev, G. A. Lalazissis, and P. Ring, Phys. Rep. **409**, 101 (2005).

[9] P. Ring, Prog. Part. Nucl. Phys. **37**, 193 (1996).

[10] P. G. Reinhard, Rep. Prog. Phys. **52**, 439 (1989).

[11] M. Bender,K. Rutz, P. G. Reinhard, J. A. Maruhn, and W. Greiner, Phys. Rev. **C 60**, 034304 (1999).

[12] R. J. Furnstahl, R. Gaulam, and S. Thomas, Ann. Rev. Nucl. Part. Sci. **58**,(2008).

[13] A. V. Afanasjev, and H. Abusara, Phys. Rev. **C 81**, 014309 (2010).

[14] J. N. Ginocchio, Phys. Rev. Lett. **78**, 436 (1997).

[15] P. J. Twin, B. M. Nyakó, A. H. Nelson, J. Simpson, M. A. Bentley, H. W. Cranmer-Gordon, P. D. Forsyth, D. Howe, A. R. Mokhtar, J. D. Morrisson, J. F. Sharpey-Schafer, and G. Sletten, Phys. Rev. Lett. **57**, 811 (1986).

[16] H. Abusara, A. V. Afanasjev, and P. Ring, Phys. Rev. **C 82**, 044303 (2010).

[17] A. V. Afanasjev, and H. Abusara, Phys. Rev. **C 78**, 014315 (2008).

[18] H. Abusara, and A. V. Afanasjev, Phys. Rev. **C 79**, 024317 (2009).

[19] G. A. Lalazissis, P. Ring, and Rom. Journ. Phys., Vol. **58**, Nos 9-10, (2013)

[20] H. Abusara, Phys. Conf. Series, 869 (2017)

[21] J. D. Walecka, Ann. Phys, N. Y. **83**, 491 (1974).

[22] B. D. Serot, and J. D. Walecka, Adv. Nucl. Phys. **16**, 1 (1986)

[23] Y. K. Gambhir, P. Ring, and A. Thimet, Ann. Phys. **198**, 132 (1990).

[24] J. Boguta, and A. R. Bodmer, Nucl. Phys. **A292**, 413 (1977).

[25] P. G. Reinhard, M. Rufa, J. Maruhn, W. Greiner, and J. Friedrich, Z. Phys., **A323**, 13 (1986).

[26] W. Long, J. Meng, N. V. Giai, and S. G. Zhou, Phys. Rev. **C 69**, 034319 (2004).

[27] B. G. Todd-Rutel, and J. Piekarewicz, Phys. Rev. Lett. **95**, 122501 (2005).

[28] R. Brockmann, and J. Frank, Phys. Rev. Lett. **68**, 1830 (1992).

[29] Niksic, D. Vretenar, P. Finelli, and P. Ring, Phys. Rev. **C 66**, 024306 (2002).

[30] X. Roca-Maza, X. Viñas, M. Centelles, P. Ring, and P. Schuck, Phys. Rev. **C 84**, 054309 (2011).

[31] A. Bohr, and B. R. Mottelson, Nuclear Structure Vol.II, W. A. Benjamin, (1975).

[32] Shuichiro Ebata, and Takashi Nakatsukasa, Phys. Scr. **92**, 064005 (2017)

[33] W. Nazarewicz, Nucl. Phys. **A520-333c**, (1990).

[34] R.J.Blin-stoyle, Nuclear and Particle Physics, Chapman and Hall, New Delhi,(1991).

[35] L. P. Gaffney et.al., Nature **497**, 199 (2013).

[36] I. Dutt, and P. Mukherjee, Phys. Rev. **C 124**, 888 (1961).

[37] L. M. Robledo, and G. F. Bertsch, Phys. Rev. **C 84**, 054302(2011).

[38] A. Gyurkovich, A. Sobiczewsk,B. Nerlo-pomorska and K. Pomorski,Phys. Lett. **105B** (1981)

[39] L. M.Robledo, and R. R Rodríguez-Guzma, Jour.Phys,(2012).

[40] P. Ring,Nucl. phys. vol 37, (1996).

[41] Michael Bender, Paul-Henri Heenen, and Paul-Gerhard Reinhard, Rev. Mod. Phys, (2003).

[42] S. K. Patra, Phys. Rev. **C 48, 1449 (1993).**

[43] M. A. Preston, and R. K. Bhaduri, Structure of Nucleus, Addison-Wesley Publishing Company, Ch.8, page 309 (1982).

[44]]. P. Möller, and J. Nix, Nucl. Phys. **A 536**, 20 (1992)

[45] Shan-Gui Zahou, Physica Scripta **91**, 063008 (2016).

[46] V. De Donno,G. Co, M. Anguiano, and A. M. Lallena, Phys. Rev. **C 95**, 054329 (2017).

[47] Chong Qi, and Tao Chen, Phys. Rev. **C 92**, 051304 (2015)

[48] P. Ring, and P. Schuck, The Nuclear Many-Body Problem, (Springer-Verlag, Berlin), (1980).

[49] V. G. Soloviev, A. V. Sushkov, and N. Yu. Shirikova, Phys. Part. Nucl. **25**, 377 (1994).

[50] J. Boguta, and A. R. Bodmer, Nucl. Phys. **A 1977**, 292 (1996).

[51] G. A. Lalazissis, S. Karatzikos, R. Fossion, D. Peña Arteaga, A. V. Afanasjev, and P. Ring, Phys. Lett. **B 671**, 36 (2009).

[52] G. A. Lalazissis, J. König, and P. Ring, Phys. Rev. **C 55**, 540 (1997).

[53] G. A. Lalazissis, T. Nikšić, D. Vretenar, and P. Ring, Phys. Rev. **C 71**, 024312 (2005).

[54] A. Staszack, M. Stoitsov, A. Baran, and W. Nazarewicz, Eur. Phys. Journ. **A 46**, 85 (2010).

[55] https://www.radiochemistry.org/periodictable/elements/isotopes_data/62.html

[56] M. Wang, G. Audi, A. H. Wapstra, et.al, Chinese Physics **C 36**, 1603 (2012).

[57] L. R. B. Elton, Nuclear Sizes, Oxford University Press, Oxford, (1961).

[58] I. Angeli,K. P. Marinova, Atomic data and nuclear data tables, Elsevier, pg 185-206, (2013).

[59] K. Nomara, D. Vretenar,T. Nikšić, and Bing-Nan Lu, Phys. Rev. **C 89**,024312 (2014).

[60] W. Zhang, Z. P. Li, S. Q. Zhang, and J. Meng, Phys. Rev. **C 81**, 034302 (2010).

[61] Y. El-Bassem, and M. oulne, Int. Jour. of Mod. Phys,E Vol. **24**, 1550073 (2015).

[62] H. Abusara, A. V. Afanasjev, and P. Ring, Phys. Rev. **C 85**, 024314 (2012).

[63] P. A. Butler, and W. Nazarewicz, Rev. Mod. Phys. **68**, 349 (1996)

[64] P. Ring, Progress in Particle and Nuclear Physics, vol **37(10)**, 193-263, (1996).

[65] A. V.Afanasjev,and P. Ring,Physics reports, **409(3)**, 101-259, (2000).

[66] G. A. Lalazissis, T. Niki, D. Vretenar, and P. Ring, Phys. Rev. **C 71**, 024312 (2005).

[67] P. A. Butler, and W. Nazarewicz Rev. Mod. Phys. **68**, 349 (1996).

[68] P. Möller, J. R. Nix, W. D. Myers, and W. J. Swiatecki, At. Data ucl. Data Tables **59**, 185 (1995).

[69] D. G. Madland, and J. R. Nix, Nucl. Phys. **A476**, 1 (1981).

[70] P. Möller and J. R. Nix,At. Data and Nucl. Data Tables 39, 213 (1988).

[71] G. A. Lalazissis, M. M. Sharma, P. Ring, Nucl. Phys. **A597**, 35 (1996).

[72] K. Pomorskiet al., Nucl. Phys. **A624**, 349 (1997).

[73] P. A. Butler, and W. Nazarewicz, Rev. Mod. Phys. **68**, 349(1996).

[74] B. Singh, R. Zywina, and R. B. Firestone, Nucl. Data Sheets **97**, 241 (2002).

[75] G. A. Lalazissis, S. Karatzikos, R. Fossion, D. P. Arteaga, A. V. Afanasjev, and P. Ring, Phys. Lett. **B671**, 36 (2009).